Research, Society and Development, v. 11, n. 8, e22911830790, 2022
(CC BY 4.0) | ISSN 2525-3409 | DOI: http://dx.doi.org/10.33448/rsd-v11i8.30790

Study of drying kinetics in ceramic plates with the addition of diatomite tailings

Estudo da cinética de secagem em placas cerâmicas com adição de rejeitos de diatomita

Estudio de cinéticas de secado en placas cerámicas con adición de relaves de diatomeas

Received: 05/23/2022 | Reviewed: 06/11/2022 | Accept: 06/15/2022 | Published: 06/17/2022

Raniere Fernandes Costa
ORCID: https://orcid.org/0000-0002-5831-4251
Universidade Federal de Campina Grande, Brazil
E-mail: ranierengenharia.costa@gmail.com
Alysson Dantas Ferreira
ORCID: https://orcid.org/0000-0003-0029-8364
Universidade Federal de Campina Grande, Brazil
E-mail: alysson.dantas@eq.ufcg.edu.br
José Jefferson da Silva Nascimento
ORCID: https://orcid.org/0000-0002-2620-6491
Universidade Federal de Campina Grande, Brazil
E-mail: jeffpesquisador@gmail.com
Maria Luiza de Souza Rezende
ORCID: https://orcid.org/0000-0002-6189-9924
Universidade Federal de Campina Grande, Brazil
E-mail: mluizarezende@hotmail.com
José Jorge da Silva Junior
ORCID: https://orcid.org/0000-0003-4497-5689
Universidade Federal de Campina Grande, Brazil
E-mail: josejorge_18@hotmail.com
Antônio Nunes de Oliveira Vieira
ORCID: https://orcid.org/0000-0001-5697-8110
Instituto Federal do Ceará, Brazil
E-mail: nunes.vieira@ifce.edu.com

Abstract
The drying process of ceramic bricks plays a key role in the amount of water available both inside the material and on its surface. This work aimed to analyze drying kinetics on ceramic tiles with different percentages of diatomite tailings, which was experimentally carried out in an oven with forced air circulation. To this end, laboratory tests were performed using different samples in which the drying kinetics was evaluated considering different environmental conditions (temperature and relative humidity), based on a 2^k factorial experimental design with three factors: the drying temperatures (333 and 383 K), the homogeneity of the mixture (30 and 60 min) and the percentage of the tailings (10 and 30%). From the results matrix, some models of drying kinetics were adjusted to the experimental data, having the Page model presented the best result. Still in possession of the results matrix, a regression model was applied to obtain equations that describe Page's fit parameters. The drying curves developed from the estimated parameters, presented a significant agreement with the experimental data, being validated within a 99% confidence interval.
Keywords: Drying; Estimated parameters; Experimental design.

Resumo
O processo de secagem dos tijolos cerâmicos desempenha um papel fundamental na quantidade de água disponível tanto no interior do material quanto em sua superfície. Este trabalho teve como objetivo analisar a cinética de secagem de revestimentos cerâmicos com diferentes porcentagens de rejeitos de diatomita, que foi realizado experimentalmente em estufa com circulação forçada de ar. Para tanto, foram realizados ensaios laboratoriais em diferentes amostras nas quais a cinética de secagem foi avaliada considerando diferentes condições ambientais (temperatura e umidade relativa), com base em um delineamento fatorial 2^k com três fatores: as temperaturas de secagem (333 e 382 K), a homogeneidade da mistura (30 e 60 min) e a porcentagem de rejeitos (10 e 30%). A partir da matriz de resultados, alguns modelos de cinética de secagem foram ajustados aos dados experimentais, sendo que o modelo de Page apresentou o melhor resultado. Ainda de posse da matriz de resultados, aplicou-se um modelo de regressão para obter equações que descrevem os parâmetros de ajuste de Page. As curvas de secagem desenvolvidas a partir dos parâmetros estimados apresentaram concordância significativa com os dados experimentais, sendo validadas dentro de um intervalo de confiança de 99%.
Palavras-chave: Secagem; Parâmetros estimados; Design experimental.

Resumen
El proceso de secado de los ladrillos cerámicos juega un papel fundamental en la cantidad de agua disponible tanto en el interior del material como en su superficie. Este trabajo tuvo como objetivo analizar la cinética de secado sobre baldosas cerámicas con diferentes porcentajes de relaves de diatomeas, el cual se realizó experimentalmente en un horno con circulación de aire forzado. Para ello, se realizaron ensayos de laboratorio con diferentes muestras en las que se evaluó la cinética de secado considerando diferentes condiciones ambientales (temperatura y humedad relativa), a partir de un diseño experimental factorial 2^k con tres factores: las temperaturas de secado (333 y 383 K), la homogeneidad de la mezcla (30 y 60 min) y el porcentaje de los relaves (10 y 30%). A partir de la matriz de resultados, se ajustaron algunos modelos de cinética de secado a los datos experimentales, siendo el modelo de Page el que presentó el mejor resultado. Todavía en posesión de la matriz de resultados, se aplicó un modelo de regresión para obtener ecuaciones que describan los parámetros de ajuste de Page. Las curvas de secado desarrolladas a partir de los parámetros estimados, presentaron una concordancia significativa con los datos experimentales, siendo validadas dentro de un intervalo de confianza del 99%.
Palabras clave: Secado; Parámetros estimados; Diseño experimental.

1. Introduction

The Brazilian ceramic industry stands out for the number of activities incorporated into its production cycle and, from the social point of view, for its labor absorption capacity. Red ceramics have a high capacity to incorporate tailings into the clay without detriment to the technological properties of the final product, besides being a good alternative for the reuse of mineral tailings. One of these materials is diatomite, also called diatomous earth, a biogenic sedimentary rock with high content of natural amorphous silica and small amounts of residual minerals (Macedo et al., 2020; Letelier, 2016), which generates a large amount of tailings in its beneficiation process. Most of the amorphous silica is in the form of diatomaceous frustules and, secondarily, in the form of sponge spicules and flagellated skeletons of silicone. This type of SiO_2 can react with $Ca(OH)_2$ and produce hydrated calcium silicate (CSH). Porous loads such as diatomite produce good levels of resistance due to more efficient mechanical adhesion and even diffusion of macromolecules in load structure. Among its advantages, diatomite differs from other minerals by having excellent mechanical properties such as hardness, corrosion and wear resistance, resistance to chemical attack, low mass density, durability in environments, aggressiveness and high-temperature stability (Ferrer, 2013). The foregoing has made these materials the subject of research in recent years with the aim of optimizing their properties and enhancing their uses (Qiu et al., 2017). Some studies have already demonstrated the potential of incorporating diatomite in the manufacture of ceramic materials.

Macedo et al. (2020) have studied the addition of diatomite in concrete production, reaching the following conclusions: the diatomite studied was considered pozzolanic, presenting a pozzolanic activity index of 650 mg of $Ca(OH)_2$ / g of diatomite, wherein the active silica reacted with the calcium hydroxide present in the cement, forming hydrated silicates and galandin, increasing the concrete's compressive force; the addition of diatomite to concrete, in spite of its porous microstructure, does not significantly alter concrete's porosity and water absorption; the studied diatomite, however, improved concrete's physical and mechanical properties. The best results were obtained for the concrete formulated with a 10% by weight addition of diatomite.

Betsuyaku (2015) demonstrated that the addition of diatomaceum sand in the manufacture of ecological bricks in samples D1 (5% residue in soil replacement), D2 (10% residue in soil replacement), NDC 01 (5% of residue in cement replacement) and NDS 01 (10% residue in soil replacement + cement), presented satisfactory results in its use as non-structural closure material in place of conventional masonry, resistance above 1.7 MPa, as recommended by NBR 10834, after the 28-day curing period.

The occurrence of pathologies in buildings is usually associated with the presence of moisture, which may result from the presence of water in the material or in the building element, or from its evaporation.

The manufacturing process of ceramic products comprises the following stages: exploration of the quarries, previous treatment of the raw material, homogenization (mixing with water to give plasticity to the raw material), drying and firing (Nascimento, 2020). Among the mentioned stages, drying is one of the most important ones in the manufacturing process. It is a thermodynamic process, in which water—previously added in the homogenization stage—is withdrawn from the product by evaporation (Lima, 2017). The drying process therefore plays a key role in the amount of water available, both inside the material and on its surface (Barreira, 2015).

The drying method in ceramic bricks is important for improving the properties of materials and enhancing efficiency and reducing costs in the process. Likewise, the type of material to be dried and the drying time are also important factors to be analyzed in order to optimize the drying process by increasing the productivity of the equipment used and reducing energy consumption, thus improving the quality of the final product. Drying quality can be affected by temperature, humidity, and hot air speed, as well as drying time. When temperature, relative humidity, and hot air speed are equal, drying time is vital for brick properties. In the drying process, moisture is evaporated and the physical and mechanical properties of the brick are altered (Lu, 2016).

It is currently considered that the first stage of the drying process is controlled by liquid or vapor diffusion mechanisms. Thin layer models are used in the study of drying, which assume a layer of material sufficiently thin for the external air conditions to remain constant in the material during drying. These models are, according to the literature, distributed in three categories (Kuitche, 2007), which are theoretical, semi-theoretical and empirical, and also assume that the resistance to moisture flow is evenly distributed throughout the homogenous isotropic material. The theoretical models consider the internal resistances to the moisture flow, while the semi-theoretical and empirical models reflect only external resistances to the moisture transfer between the material and the air.

The present work aims to analyze empirical equations widely disseminated in the literature, seeking to identify the one that best describes the drying kinetics in ceramic plates made of clay and diatomite tailings for the studied compositions. Once the best-fitting model is obtained, we will derive regressed equations to estimate its fitting parameters.

2. Methodology

The ceramic plates were made from a mixture of "in natura" clay and diatomite tailings. The properties of the material, as well as its characterization, can be found in Costa et al. (2021). Both the diatomite tailings and the clay were chosen due to their high SiO_2 content. Regarding the granulometric distribution, the diatomite tailings are quite thin, ensuring a good contact surface for the reaction medium, thus participating more actively in the reaction.

Both the tailings and the clay were crushed and mechanically sieved to a passing fraction of 80 mesh. Then, homogenization was performed in a ball mill for 30 and 60 min, adding 8% moisture to the masses—enough to obtain a good homogenization and reach the plastic point needed for conformation. Samples were prepared with 10 and 30% of their mass composed of diatomite tailings. The ceramic plates were molded by uniaxial pressing in a hydraulic press, using a steel matrix and pressure of 20 Mpa, in semi-dry mass, with dimensions of 60 x 20 x 5 mm^3, weight of 11.82 g and density of 1.97 g/cm^3, as suggested by Medeiros et al. (2014).

Drying of the samples

The drying of the ceramic plates was carried out in an oven (model Marconi brand) with air circulation, with temperature controller and with an operating range between 273 and 473 K. A galvanized wire tray was used to accommodate the samples in order to facilitate air circulation above them inside the oven (Figure 1).

Figure 1 – Tray and ceramic plates with dimensions in millimeters.

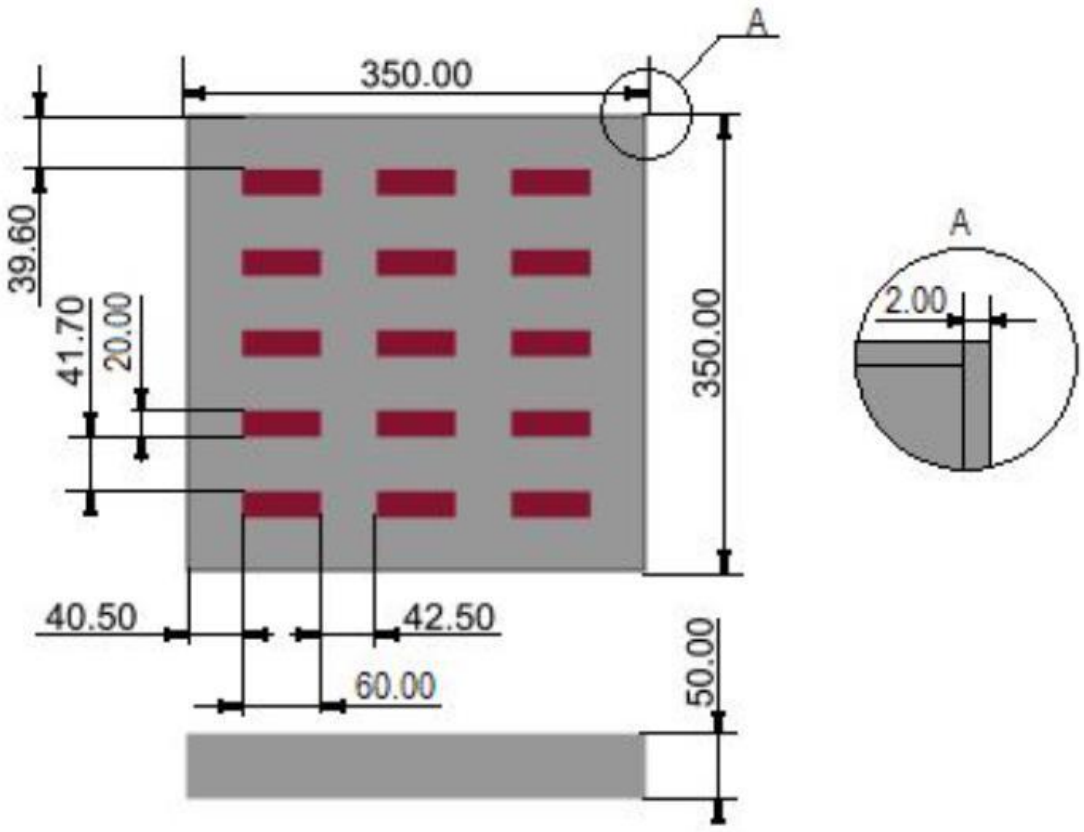

Source: Authors.

The first step of each experiment was to weigh the samples and measure their lengths at 10-minute intervals during the first hour of drying, with the rest of the measurements being taken at 30-minute intervals until the mass variation stagnated. At the end, in order to obtain the dry mass, the samples were taken to a drying and sterilization (FANEM) without air circulation at 383 K for 48 hours, according to the methodology used by Nascimento (2002) and Santana (2006). The masses of the samples were obtained by means of an electronic balance with an accuracy of ± 0.01g; the dimensions of the samples were measured using a digital pachymeter with an accuracy of ± 0.01mm, and the relative humidity was verified by means of a hygrometer. The temperature was measured at the fixed center of each sample, using a thermal gun (model TI 890) with a scale ranging from -223 to 1273 K. Drying was performed in triplicate, each experiment containing five samples of ceramic bricks, and the process conditions followed a 2^k. The experiment matrix is presented in Table 1.

Table 1 – Experiment matrix of the 2^k factorial design.

	P [%]	T [K]	H [min]
Experiment 1	10	383	30
Experiment 2	10	383	60
Experiment 3	10	333	30
Experiment 4	10	333	60
Experiment 5	30	383	30
Experiment 6	30	383	60
Experiment 7	30	333	30
Experiment 8	30	333	60

Source: Authors.

Drying kinetics modeling

From the data of mass loss of the samples during drying, the moisture content was calculated from Equation 1:

$$MR = \frac{M_d - M_e}{M_0 - M_e} \quad (1)$$

in which M_d is the moisture content at time t, Mo is the initial moisture content, and Me is the equilibrium moisture content, all given in kilograms of water per kilogram of dry matter.

Knowing the moisture contents over time, we constructed the drying curves for each replica of the scenarios presented in Table 1. The Levenberg-Marquardt algorithm was used to obtain the experimental fitting parameters for the models presented in Table 2, thus minimizing the error between the experimental data and the theoretical curves.

Table 2 – Mathematical models used to describe the drying process.

Model	Equation	References
Newton	MR = exp(-ct)	Henderson, 1974
Page	MR = exp(-dt^p)	Guarte, 1996
Henderson and Pabis	MR = a exp(-bt)	Zhang and Litchfield, 1991

Source: Authors.

The model that best fit the experimental data was determined using the statistical parameters of the highest value of the coefficient of determination R^2, the lowest values of the chi-squared (χ^2), and the root mean square error (RMSE). The equations for these statistical tests are presented in Equations 2, 3, and 4, respectively.

$$R^2 = 1 - \left[\frac{\sum_{i=1}^{N}(MR_{pre,i} - MR_{exp,i})^2}{\sum_{i=1}^{N}(\overline{MR}_{pre} - MR_{exp,i})^2}\right] \quad (2)$$

$$\chi^2 = \frac{\sum_{i=1}^{N}(MR_{exp,i} - MR_{pre})^2}{n - N} \quad (3)$$

$$RMSE = \left[\frac{1}{N}\sum_{i=1}^{n}\left(MR_{exp,i} - MR_{pre,i}\right)\right]^{\frac{1}{2}} \quad (4)$$

In the equations above, $MR_{pre,i}$ is the i-th relative humidity obtained from the model, $MR_{exp,i}$ is the i-th relative humidity obtained from the experimental data, N is the number of observations and n is the number of constants estimated from the experimental data.

3. Results and discussion

Drying kinetics

The drying process was performed as described in the materials and methods section. From the three replicates performed, the average mass loss of the samples for each of the experiments was calculated and then converted into moisture content with the help of Equation 1. The result of the average moisture content for each experiment over time is shown in Figure 2.

Figure 2 – Drying curves of the experiments performed.

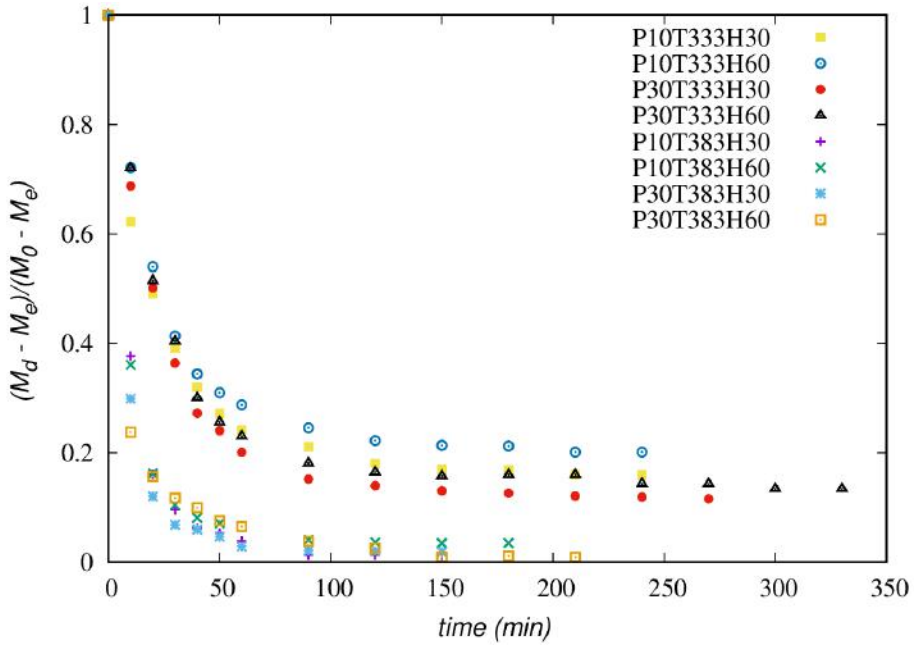

Source: Authors.

Figure 2 shows the behavior of the moisture content for all eight experiments described in Table 1. In it, we can observe the influence of each of the parameters analyzed, making clear the influence of temperature during the drying process. The first four curves represent drying at 333 K, whereas the other curves represent drying at a temperature of 383 K. This behavior shows us that temperature is the main factor in speeding up or slowing down the drying time, since the 383 K curves reach lower moisture contents in the samples when the same period of time is considered. A second conclusion that we can

infer, still on temperature, is that 333 K were not enough to remove all moisture from the samples, since moisture contents stabilized close to 20%.

As for the effect of the percentage of diatomite tailings present in the sample, we can observe that the 30% tailings curves reach lower moisture contents than the 10% curves, leading to the conclusion that increasing the percentage of tailings from 10 to 30% facilitated the outflow of moisture from the ceramic bricks. Costa et al. (2021) studied the effect of mass homogenization using diatomite tailings in ceramic plates, observing that the longer the material homogenization time, the less water is lost during drying.

After obtaining the drying curves for each experiment in Table 1, we proceeded to fit the experimental coefficients for the equations presented in Table 2. The degree of agreement between the analyzed models and the experimental data was evaluated and is presented next in Tables 3, 4, and 5.

Table 3 shows the statistical parameter values of the coefficient of determination (R^2) for the Newton, Page, and Henderson models. This test shows the degree of fitting of the evaluated models to the experimental data. By averaging the results over all 24 experiments, we found that the Page model is more representative than Newton's and Henderson's, averaging 95.6%, while the Newton and Henderson models averaged 78% and 78.57%, respectively.

Table 3 – Results of the coefficient of determination test (R^2).

	R^2								
	Newton			*Page*			*Henderson*		
	Rep1	*Rep2*	*Rep3*	*Rep1*	*Rep2*	*Rep3*	*Rep1*	*Rep2*	*Rep3*
Exp. 1	*98,85*	99,09	97,72	*99,49*	99,75	99,45	*98,71*	98,99	97,46
Exp. 2	*93,06*	96,58	94,42	*97,52*	99,08	97,98	*92,42*	96,24	93,86
Exp. 3	*60,14*	30,68	28,19	*94,80*	95,00	91,82	*61,75*	38,73	31,78
Exp. 4	*48,94*	53,28	49,39	*92,38*	90,67	91,69	*53,95*	56,77	53,87
Exp. 5	*97,48*	97,6	98,38	*99,19*	99,44	99,50	*97,18*	97,36	98,19
Exp. 6	*85,09*	90,92	94,48	*98,85*	98,26	98,58	*83,78*	90,12	94,00
Exp. 7	*75,22*	83,85	81,31	*91,94*	93,54	92,19	*74,42*	83,29	80,50
Exp. 8	*71,78*	74,28	68,52	*91,45*	91,24	90,93	*71,01*	73,47	67,86
Avg.	*78,82*	78,29	76,89	*95,70*	95,87	95,27	*79,15*	79,37	77,19

Source: Authors.

Table 4 shows the results of the chi-square statistical tests (χ^2) for Newton, Page, and Henderson models. This analysis qualitatively evaluates the relationship between the experimental results and the results presented by the models, so that the lower the test value, the better the response of the evaluated model. Therefore, by averaging the results of all 24 experiments, we can see that the Page model also achieved the best results in this test.

In Table 5 we can find the results of the root mean squares statistical tests (RMSE) for the Newton, Page, and Henderson models. In these results, we get the sum of the differences between the values estimated by the model and the data obtained from the experiment, and this difference is squared. Similarly to the chi-square test, the lower the test value, the better the response of the evaluated model. From the above, we found the Page model to have the lowest value for the squared sum of the tailings, thus indicating a better fit in comparison to the Newton and the Henderson models.

As shown in Tables 3, 4, and 5, we notice that the Newton and Henderson models presented close results among them; however, the model that showed the best fit to the experimental data evaluated was Page's. This model was chosen to represent the drying kinetics of bricks with diatomite tailings.

As shown in Table 2, the Page model implies the need to estimate two fitting parameters, which were found by applying the Levenberg-Marquardt algorithm. These parameters were obtained for the experiments presented in Table 1, and their values for each replicate are shown in Table 6.

In any experimental design, it is always recommended to examine the residues and check for violations of basic assumptions that could invalidate the results. Montgomery (2016) recommends analysis of variance, noting whether the data show a normal distribution behavior and whether they are independently distributed. These assumptions must be verified by analyzing the graphs of the residues.

Table 4 – Results of the chi-square statistical test.

	χ^2								
	Newton			*Page*			*Henderson*		
	Rep1	*Rep2*	*Rep3*	*Rep1*	*Rep2*	*Rep3*	*Rep1*	*Rep2*	*Rep3*
Exp. 1	*0,0007*	*0,0004*	*0,0012*	0,0003	0,0001	0,0003	0,0007	0,0005	0,0013
Exp. 2	*0,0025*	*0,0013*	*0,0020*	0,0009	0,004	0,0007	0,0027	0,0014	0,0022
Exp. 3	*0,0119*	*0,0149*	*0,0154*	0,0016	0,0011	0,0018	0,0114	0,0132	0,0146
Exp. 4	*0,0175*	*0,0174*	*0,0180*	0,0026	0,0035	0,0026	0,0158	0,0161	0,0164
Exp. 5	*0,0012*	*0,0010*	*0,0006*	0,0004	0,0002	0,0002	0,0013	0,0011	0,0007
Exp. 6	*0,0028*	*0,0021*	*0,0014*	0,0002	0,0004	0,0004	0,0030	0,0023	0,0015
Exp. 7	*0,0091*	*0,0066*	*0,0073*	0,0030	0,0026	0,0031	0,0094	0,0068	0,0282
Exp. 8	*0,0119*	*0,0104*	*0,0123*	0,0036	0,0035	0,0036	0,0122	0,0107	0,0126
Avg.	*0,0072*	*0,0068*	*0,0068*	0,0016	0,0015	0,0016	0,0071	0,0065	0,0097

Source: Authors.

Table 5 – Results of the RMSE statistical test.

	RMSE								
	Newton			*Page*			*Henderson*		
	Rep1	*Rep2*	*Rep3*	*Rep1*	*Rep2*	*Rep3*	*Rep1*	*Rep2*	*Rep3*
Exp. 1	*0,0257*	*0,0204*	*0,0342*	0,0172	0,0107	0,0168	0,0271	0,0215	0,0361
Exp. 2	*0,0496*	*0,0361*	*0,0443*	0,0297	0,0188	0,0267	0,0519	0,0378	0,0465
Exp. 3	*0,1090*	*0,1223*	*0,1241*	0,0936	0,0328	0,0419	0,1068	0,1149	0,1209
Exp. 4	*0,1324*	*0,1220*	*0,1342*	0,0511	0,0590	0,0544	0,1257	0,1270	0,1282
Exp. 5	*0,0339*	*0,0313*	*0,0248*	0,0192	0,0153	0,0139	0,0359	0,0331	0,0263
Exp. 6	*0,0526*	*0,0455*	*0,0377*	0,0146	0,0199	0,0191	0,0549	0,0475	0,0393
Exp. 7	*0,0955*	*0,0811*	*0,0857*	0,0544	0,0513	0,0554	0,0970	0,0825	0,0875
Exp. 8	*0,1090*	*0,1018*	*0,1111*	0,0600	0,0594	0,0595	0,1104	0,1034	0,1122
Avg.	*0,0760*	*0,0713*	*0,0745*	0,0425	0,0334	0,0360	0,0762	0,0710	0,0746

Source: Authors.

Table 6 – Page's fit parameter values.

	d [s^-1]			*p [ ]*		
	R1	*R2*	*R3*	*R1*	*R2*	*R3*
Exp. 1	*0,1645*	*0,1700*	*0,2296*	0,7695	0,7846	0,6616
Exp. 2	*0,3410*	*0,2704*	*0,2939*	0,5161	0,6144	0,5680
Exp. 3	*0,1996*	*0,2110*	*0,2383*	0,4525	0,4219	0,4021
Exp. 4	*0,1877*	*0,1716*	*0,1896*	0,4302	0,4460	0,4266
Exp. 5	*0,3056*	*0,3200*	*0,2667*	0,6053	0,6030	0,6760
Exp. 6	*0,4280*	*0,3293*	*0,2620*	0,4579	0,5324	0,6098
Exp. 7	*0,1753*	*0,1418*	*0,1524*	0,4945	0,5538	0,5368
Exp. 8	*0,1877*	*0,1796*	*0,1904*	0,4535	0,4703	0,4471

Source: Authors.

We can verify the assumption of normality through the normal probability plots shown in Figure 3.

Figure 3 – Normal probability plot a) d and b) p.

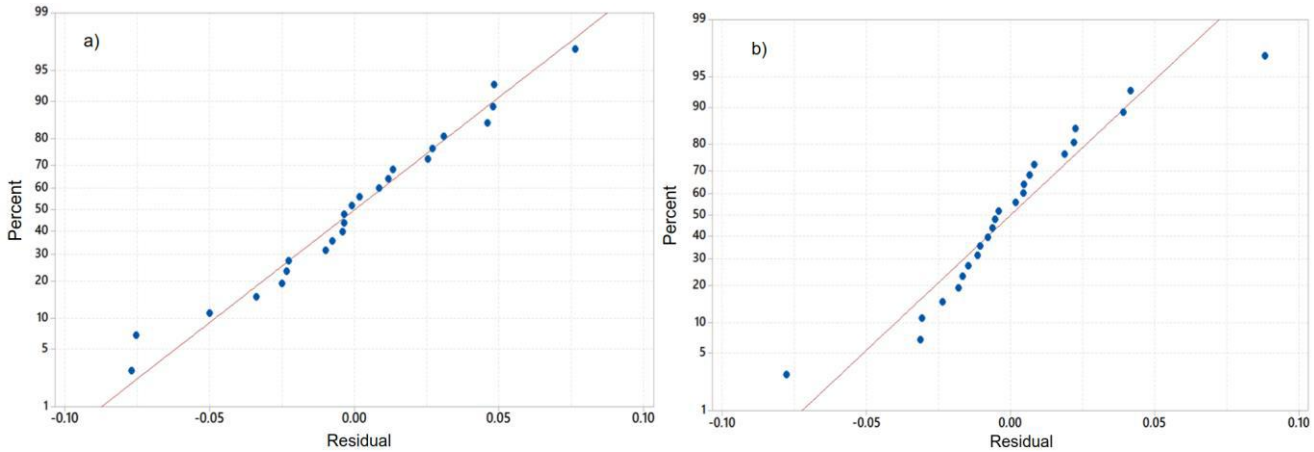

Source: Authors.

Analyzing the normal probability plots for parameters d and p of the Page model, we find that in the plot for parameter p, the experimental data points follow the fitted distribution line, indicating that the normal distribution might be a good fit for the data. As for the d parameter plot, we also find that most of the experimental data points follow the normal distribution line, but the points at the ends of the x-axis are some distance away, suggesting a distribution with two outlier points. Therefore, we can conclude that both parameter d and p exhibit normal behavior, thus meeting Montgomery's (2016) recommendation for observations to be normal.

By plotting the residues versus the fitted values (Figure 4), we can verify the assumption of independent distribution of variance.

Figure 4 – Plot of residues versus fitted values a) d and b) p.

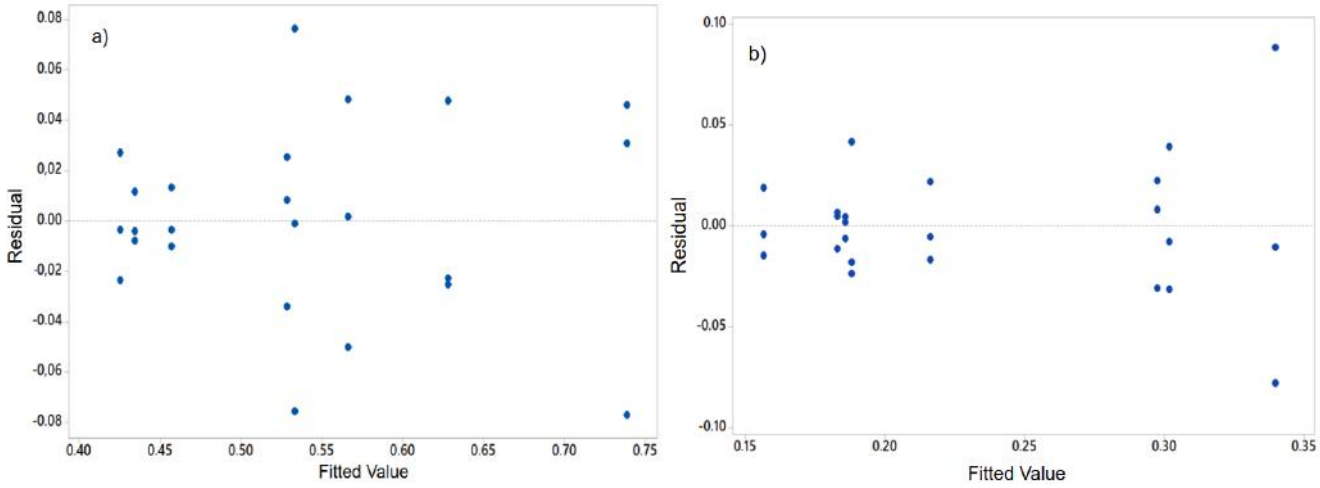

Source: Authors.

Now studying the plots of residues versus the fitted values of parameters d and p, we notice in both plots that the points are randomly distributed on both sides of the line and with no recognizable patterns, indicating that the variance considers the observations to be independently distributed, as recommended by Montgomery (2016).

Based on the estimated values of parameters d and p, and once analysis of variance showed that observations were normal and independently distributed, Equations 5 and 6 were developed by fitting a regression model to the data, in order to estimate parameters d and p as a function of diatomite tailings mass percentage, drying temperature and homogenization of the material.

$$d = 0{,}703 - 0{,}02432P - 0{,}00654T - 0{,}01072H + 0{,}000303PT + 0{,}000373PH + 0{,}000143TH - 0{,}000004PTH \quad (5)$$

$$p = -0{,}491 + 0{,}0314P + 0{,}01360T + 0{,}01203H - 0{,}000371PT - 0{,}000449PH - 0{,}000173TH + 0{,}000005PTH \quad (6)$$

We calculated the coefficient of determination (R^2) for Equations 5 and 6, obtaining a fit of 81.7% for parameter d and a fit of 87.98% for parameter p, in comparison to the data in Table 6. In order to evaluate the accuracy of the Page model, we estimated the values for parameters d and p for the conditions presented in Table 7.

Table 7 – Parameters for validation of the Page model.

	P	T	H	d	p
Validation 1	20	353	45	0,2583	0,50585
Validation 2	10	333	30	0,2249	0,4212
Validation 3	30	383	60	0,4339	0,4845

Source: Authors.

With the estimated values of d and p, and with the help of the Page equation, the drying curves were built for the conditions presented in Table 7. The results of the proposed model were compared with experimental data, plotting a 99% statistical confidence interval as presented in Figure 5.

Figure 5 – Drying curves constructed from the proposed model (P20T353H45).

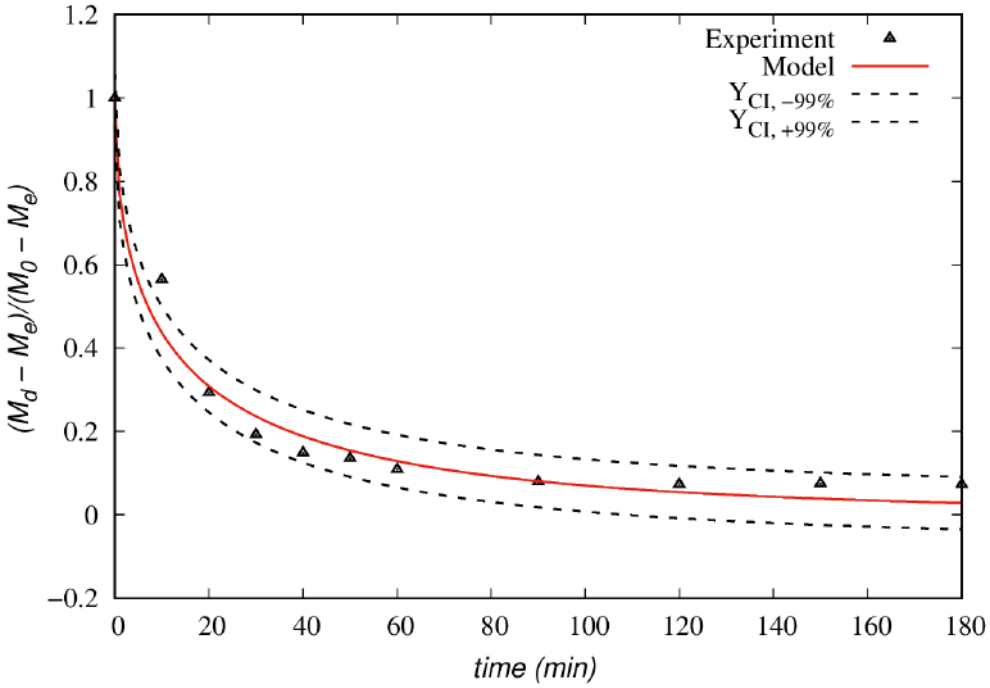

Source: Authors.

Figure 5 represents the curve of validation 1, in which the parameters of diatomite percentage, drying temperature, and homogenization time are at the center point of the experimental design. Analyzing the graph, we can observe that the curve generated by the Page model, with the experimental coefficients estimated from Equations 5 and 6, presented a good approximation when compared to the experimental data. Most of the experimental points were within the confidence interval, with only the second point deviating slightly from the curve, which may indicate an error occurred during the experiment.

Figure 6 – Drying curves built from the proposed model a) P10T333H30 and b) P30T383H60.

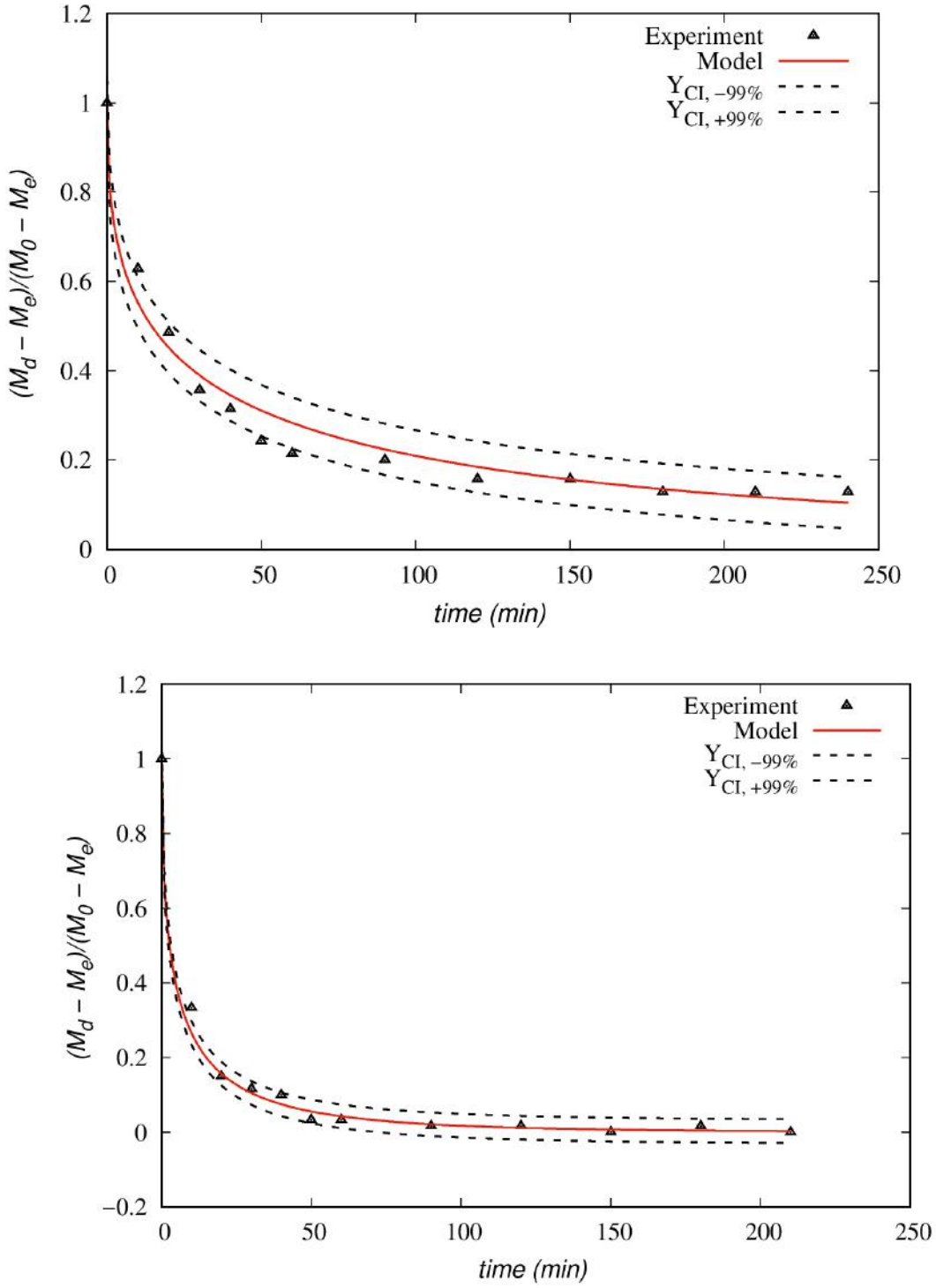

Source: Authors.

Figure 6-a shows the curve of validation 2, while Figure 6-b shows the curve of validation 3. These points were chosen because they represent the lowest and the highest values for the factors evaluated in the experimental design. Analyzing the graphs, we can see that all plots are within or on top of the lines that draw the confidence intervals, indicating that the Page model, with the experimental coefficients estimated by Equations 4 and 5, showed a good approximation when compared to the experimental data.

4. Conclusion

Regarding the results found for drying kinetics, we could observe that among the models analyzed, the Page equation was the best fit to the experimental data, presenting the best values for R^2, χ^2, and RMSE tests.

By means of the experimental design carried out, we noticed that the variance of the experimental data was normal and independent, and thus it was possible to obtain a model for Page's two fitting parameters (d and p).

The drying curve obtained by the Page model, whose experimental coefficients were calculated by the equations developed in this research, showed good agreement with the experimental data, thus validating the models.

References

Barreira, E., Delgado, J. M. P. Q., & Freitas, V. P. (2015). Wetting and drying of building materials, drying and wetting of building materials and componentes. *Building Pathology and Rehabilitation*, 4, 51–69.

Betsuyaku, R. Y. (2015). Construção de ecotijolos com adição de areia diatomácea. *Master's thesis*, Centro Universitário de Volta Redonda.

Costa, R. F., Ferreira, A. D., Silva Junior, J. J. S., Barbosa, D. J. A., Rezende, M. L. S. & Nascimento, J. J. S. (2021). Drying of clay/diatomite hybrid ceramic plates: An experimental study. *Research, Society and Development*, 10, e13710817174.

Ferrer, M., Pena, G., & Vera, E. (2013). Estructura, porosidad y resistencia mecánica a la flexión de cerámicas porosas elaboradas con barbotinas rojas y espumas de poliuretano. *Revista Colombiana de Física*, 45(3), 214–217.

Guarte, R. C. (1996). Modelling the drying behaviour of copra and development of a natural convection dryer for production of high quality copra in the Philippines. *PhD thesis*, Hohenheim University.

Henderson, S. M. (1974). Progress in developing the thin layer drying equation. *Transactions of the ASAE*, 17, 1167–1172.

Kuitche, A., Edoun, M., & Takamte, G. (2007). Influence of pre-treatment on drying on the drying kinetic of a local okro (hibiscus ersculentus) variety. *World Journal of Dairy & Food Sciences*, 2(2), 83–88.

Lima, W. d. (2017). Transferência de calor e massa em sólidos porosos com geometria complexa via análise concentrada: modelagem e simulação. *Master's thesis*, UFCG.

Lu, Z., Zhao, C. Ma, Z., Jia, W., & Wang, M. (2016). Effects of hot air drying time on properties of biomass brick. *Applied Thermal Engineering*. 109, 487–496.

Letelier, V., Tarela, E., Munoz, P. & Moriconi, G. (2016). Assessment of the mechanical properties of a concrete made by reusing both: brewery spent diatomite and recycled aggregates. *Construction and Building Materials*, 114, 492–498.

Mâcedo, A. R. S., Silva, A. S., Da Luz, D. S., Ferreira, R. L. S., Lourenço, C. S., & Gomes, U. U. (2020). Study of the effect of diatomite on physico-mechanical properties of concrete. *Cerâmica*, 66, 50–55.

Medeiros, F., Aquino, R., Rodrigues, A., Silva, H., Dias, I., & Ferreira, H. S. (2014). Produção de tijolos maciços e placas cerâmicas de revestimento com adição de Óleo lubrificante usado. *Cerâmica Industrial*, 19, 38–45.

Montgomery, D. C. & Runger, G. C. (2016). Applied Statistics and Probability for Engineers. Boston: Wiley.

Nascimento, L. P. C., Silva, S. K. B. M., Lima, E. S. d., Magalhães, H. L. F., Lima, W. M. P. B., Gomez, R. S. & Lima, A. G. B. (2020). Drying of industrial clay ceramic bricks: a theoretical investigation using lumped models. *Research, Society and Development*, 9(11).

Nascimento, J. J. (2002). Fenômenos de difusão transiente em sólidos paralelepípedos. Estudo de caso: secagem de materiais cerâmicos. *PhD thesis*, UFPB.

Qiu, M., Chen, X., Fan, Y. & Xing, W. (2017). Ceramic membranes. *Comprehensive Membrane Science and Engineering*, 1, 270–297.

Santana, E. W. F. d. (2006). Avaliação da secagem e queima de placas cerâmicas. *Master's thesis*, UFCG.

Zhang, Q. & Litchfleld, J. B. (1991). An optimization of intermittent corn drying in a laboratory scale thin layer dryer. *Dry Technol*, 9, 383–395.